Ultrafast dynamics in the power stroke of a molecular rotary motor

Conyard, Jamie; Addison, Kiri; Heisler, Ismael A.; Cnossen, Arjen; Browne, Wesley; Feringa, B.L.; Meech, Stephen R.

Published in:
Nature Chemistry

DOI:
10.1038/NCHEM.1343

Publication date:
2012

nature chemistry

SUPPLEMENTARY INFORMATION

DOI: 10.1038/NCHEM.1343

Ultrafast dynamics in the power stroke of a molecular rotary motor

Jamie Conyard,[a] Kiri Addison,[a] Ismael A. Heisler,[a] Arjen Cnossen,[b] Wesley R. Browne,[b] Ben L. Feringa[b] and Stephen R. Meech*[a]*

[a]School of Chemistry, University of East Anglia, Norwich Research Park, Norwich NR4 7TJ, UK; [b]Stratingh Institute for Chemistry, University of Groningen, Nijenborgh 4, 9747AG Groningen, The Netherlands

Additional Experimental Information

Tables

Figures

i. Fitting Procedure

The time domain data obtained directly from the fluorescence up-conversion measurements do not provide a true representation of the decay dynamics of the measured species. The measured decay profiles are convoluted with the instrument response function. In order to determine the true decay dynamics the data are subjected to a deconvolution procedure. This requires each decay curve to be fitted to a decay function (in the present case a combination of exponential and damped harmonic oscillators, Equation 1) convoluted with the instrument response function (determined from measurements of the up-converted instantaneous Raman scattering from heptane). The best fit is obtained with an evolutionary algorithm. In order to determine the fitting quality and which function provides the best fit to the data, residual plots are generated (Figure S1). For these data, it was found that a function comprising a sum of two exponential components and two damped harmonic oscillators provided an adequate fit:

$$F(t) = \sum_{n=1}^{2} A_n e^{-t/\tau_n} + A_{\omega n} \sin\left(\omega_n t + \phi_n\right) e^{-t/\tau_{Dn}} \quad , \qquad (1)$$

where A_n and $A_{\omega n}$ are the amplitudes of the exponential and oscillatory components respectively, τ_n is the time constant of the exponential decay, ω_n is the frequency of the oscillation, ϕ_n is the relative phase and τ_{Dn} is the damping constant of the oscillation. The individual components (exponential decays and oscillations) are shown in Figure S2 along with their sum and the measured data. The same data are displayed in the frequency domain through a Fourier transform (FT, Figure S2b), where the FT of both the entire decay and the data from which the exponentially decaying part has been subtracted are shown. The time domain fit parameters for the decay curves at all measured wavelengths are listed in Table S1 and Table S2.

ii. Time Dependent Fluorescence Spectra

The fluorescence decay data exhibit a marked emission wavelength dependence, so single decay traces yield only a qualitative representation of the decay dynamics. A more complete characterisation is given by the time dependence of the entire emission spectrum. The deconvoluted fits to the time domain data, measured at a range of emission wavelengths spanning the emission profile [$D(\lambda, t)$], are normalized to the amplitude of the corresponding wavelength in the steady state fluorescence spectrum [$S_0(\lambda)$] to reconstruct the emission spectrum at a given time after excitation [$S(\lambda, t)$].

$$S(\lambda,t)=\frac{D(\lambda,t)S_0(\lambda)}{\int_0^\infty D(\lambda,t)dt}$$

The fluorescence spectrum was recovered for a log-normal fit to measured data from which the solvent background was subtracted (Figure 2). Fluorescence spectra were recorded as a function of wavelength (nm), but quantitative analysis requires an energy scale. Therefore, the emission spectra are converted to wavenumber scale (cm^{-1}). This results in the creation of a three-dimensional surface (time, wavenumber and fluorescence intensity). The time dependent evolution of the emission spectrum can then be analysed by taking time slices through this surface (10 fs slices were taken for the first picosecond). The resulting spectra were fit with a log-normal function (see Figure 3a), from which the time dependent integrated fluorescence intensity, first moment and spectral width were calculated as a function of time. The fitted spectra were used to create a contour plot representation of the temporal evolution of the emission spectrum (i.e. the 3D surface viewed down the intensity axis, see Figure 3b in main paper).

In order to ensure that the deconvolution and fitting procedures did not introduce any artefact to the data, the 3-dimensional surface analysis was also performed with the raw time domain data. These data were not subjected to the deconvolution procedure and the time-dependent emission spectra obtained from the time slices were not fit with the log-normal function. This still results in the creation of a three-dimensional surface which can also be represented by a contour plot. A comparison of the contour plots resulting from the raw data and the deconvoluted data was made (Figure S3a). The features found in the fitted data are still clearly present in the raw data. An even more direct comparison can be made by slicing the 3-dimensional surfaces along a given single frequency and overlaying the resulting time domain profile (Figure S3b).

iii. Raman Data

a Measurements. Raman spectra of **1** were recorded in the solid state at λ_{exc} 785 nm using a Perkin Elmer Raman Station at room temperature. Resonance Raman spectra were obtained at λ_{exc} 355 nm (10 mW, Cobolt Lasers) in cyclohexane and in dichloromethane solutions ($abs_{355nm} = 1$). Spectra were recorded in 10 mm quartz cuvettes and in a gravity flow cell. The laser was directed to the sample via quartz prisms and Raman scattering was collected by a 25 mm diameter plano-convex lens ($f = 10$ cm) in a 150^{o} backscattering arrangement. The collimated Raman scattering was focused by a second 2.5 cm diameter plano convex lens ($f = 6$ cm) through a long pass edge filter (Semrock) into a Shamrock300i spectrograph (Andor Technology) with a 2400 L/mm grating blazed at 300 nm and acquired with a DV420A-BU2 CCD camera (Andor Technology). The spectral slit width was set to 30 μm. Each spectrum was accumulated, typically 20 times with 5 s acquisition time. Data were recorded and processed using Solis (Andor Technology) with spectral calibration performed using the Raman spectrum of acetonitrile/toluene 50:50 (v:v). The spectra are shown in Figure S4a.

b Raman Analysis. After subtraction of the solvent background two strongly enhanced modes are observed at 316 cm^{-1} and 299 cm^{-1} (Figure S4a). Such an enhancement suggests these modes are coupled to the electronic transition and undergo nuclear displacement between ground and Franck-Condon excited state. No modes are seen at lower frequencies matching the modes observed in the excited state. The two enhanced modes have a clear correspondence with the modes in the ground state Raman at 317 and 301 cm^{-1} (Figure S4a(b)). In addition the ground state shows a strong Raman active mode at 185 cm^{-1} (matching the frequency of the less intense more slowly relaxing mode, although there is no obvious equivalent in the resonance Raman spectrum) along with a number of other low frequency modes which do not appear in the resonance Raman spectrum. The assignment of the ground state modes is made through a comparison with DFT calculations, which is shown in Figure S4b. In general the agreement between calculation and experiment is good. The greater complexity of the low frequency portion of the experimental spectrum can be ascribed to lattice modes of the crystalline sample. In Figure S4c the out-of-plane displacements near C9 obtained from the DFT calculation (Gaussian 09W at the B3LYP/cc-pVTZ)[1] are shown.

iv. Transient Absorption.

The transient absorption apparatus has been described elsewhere, and has a time resolution of 200 fs.[2] With this experiment we can measure dynamics associated with non-fluorescent states, such as relaxation on the ground potential energy surface. Preliminary data are shown in Figure S5. A rather clear transient absorption/stimulated emission (Figure S5(a)) is seen centred at 560 nm which decays with a 1.5±0.3 ps decay constant (Figure S5(b)).

v. Quantum Yield Measurements

A solution of **1** in toluene ($OD_{356} > 3$) was irradiated at 365±1 nm for 20 s intervals and the change in absorption at 475 nm was monitored. The conversion of **1** to **1′** (Figure 1) was plotted against time yielding a straight line (Figure S6). The photochemical quantum yield was determined using potassium ferrioxalate as actinometer. The quantum yield was for **1′** ← **1** was calculated to be 0.14 using:

$$\text{Photon flux} = (D \cdot V \cdot N_A) / (\Phi \cdot \varepsilon \cdot d)$$

In which D is the optical density, V is the irradiated volume, N_A is the Avogadro number, Φ is the quantum yield, ε is the molar absorptivity, and d is the pathlength of the cuvette.

Excitation λ / nm	τ_1 /ps	A_1	τ_2 /ps	A_2	$\langle\tau\rangle$ /ps
455	0.11	0.57	0.87	0.08	0.20
465	0.13	0.64	0.89	0.10	0.23
472	0.14	0.70	0.93	0.13	0.26
480	0.14	0.63	0.93	0.11	0.26
488	0.16	0.61	1.00	0.12	0.30
497	0.18	0.69	1.08	0.14	0.33
506	0.19	0.61	1.12	0.13	0.36
516	0.21	0.67	1.38	0.14	0.41
525	0.20	0.67	1.20	0.15	0.38
535	0.23	0.66	1.21	0.16	0.42
545	0.25	0.77	1.37	0.18	0.46
556	0.29	0.83	1.48	0.19	0.51
576	0.31	0.88	1.31	0.18	0.48

Table SI – Lifetime data for **1** from the two exponentially decaying components of the fit.

Excitation λ / nm	τ_{D1} / ps	$\omega_1 \pm$ 0.23/ THz	$A_{\omega 1}$	φ_1	τ_{D2} / ps	$\omega_2 \pm$ 0.32/ THz	$A_{\omega 2}$	φ_2
455	0.06	3.35	0.97	0.91	0.17	5.37	0.18	1.34
465	0.07	3.36	0.86	0.66	0.21	5.29	0.15	1.00
472	0.08	3.32	0.61	0.62	0.22	5.24	0.12	0.78
480	0.09	3.42	0.61	0.56	0.22	5.21	0.13	0.85
488	0.08	3.38	0.61	0.54	0.24	5.29	0.13	0.72
497	0.09	3.43	0.51	0.40	0.26	5.20	0.11	0.55
506	0.08	3.38	0.59	0.33	0.23	5.33	0.13	0.48
516	0.10	3.53	0.41	0.18	0.20	5.43	0.14	0.33
525	0.09	3.57	0.41	0.12	0.18	5.41	0.16	0.32
535	0.09	3.41	0.39	0.02	0.23	5.45	0.14	0.20
545	0.12	3.59	0.22	0.08	0.26	5.54	0.09	0.10
556	0.15	3.72	0.16	-0.14	0.30	5.49	0.06	0.04
576[a]	0.17	3.95	0.17	-0.60	0.27	5.70	0.06	-0.30

Table SII – Damping (τ_D), frequency (ω), amplitude (A_ω) and phase (Φ) components of the two damped oscillator functions used to fit the oscillatory part of the time domain data. The error of ± 6% in the frequency was obtained from analysing repeated experiments at selected wavelengths; the error from fitting a single data set was smaller.

[a] Error on frequency increases to ±13% because of the low overall amplitude of the oscillation at these red shifted wavelengths.

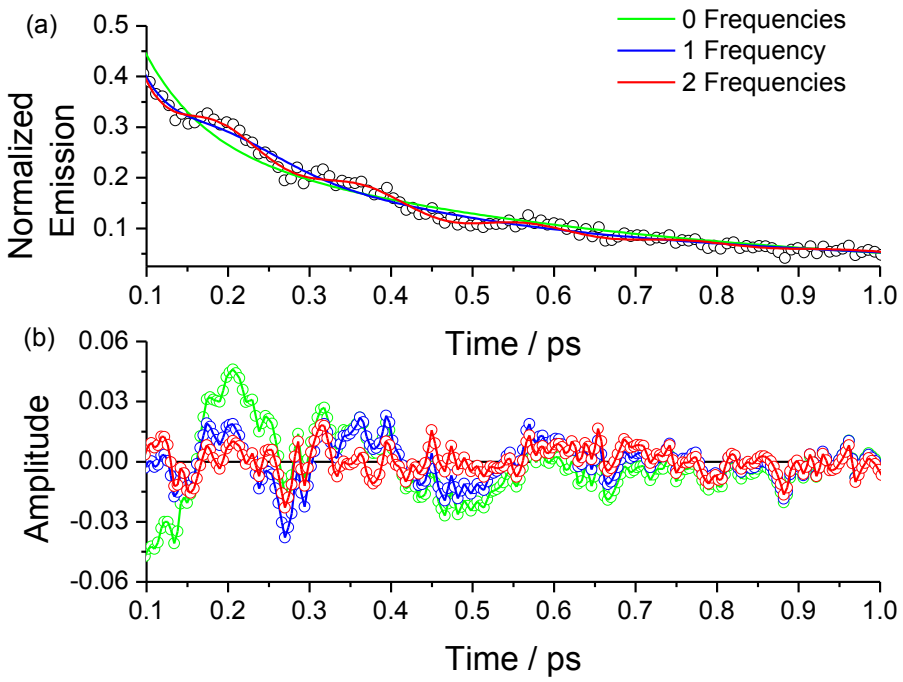

Figure S1 – A comparison of the fit quality (a) and resulting residual plots (b) obtained from fitting the time domain data (emission measured at 497 nm) with a bi-exponential only function (green), a bi-exponential combined with a single damped frequency oscillator (blue) and a bi-exponential combined with a two damped oscillator functions (red). The data is not well fit by the bi-exponential only function, where an oscillation clearly remains in the residual data, peaking at 0.2 ps, 0.35 ps and 0.6 ps (green). The combination of a single oscillator function (3.3±0.3 THz) with the bi-exponential function greatly improves the quality of the fit around the first maximum of the oscillation (0.2 ps) (blue). However, the other maxima remain poorly fit by this function. The introduction of a second oscillator results in a much better fit to the data and a nearly random residual plots (red). Attempts were made to include a third oscillator component to the fitting function at a higher frequency which resulted in a slightly improved fit and residual plot. However, the parameters associated with the previous, simpler, function were unaffected and so the simpler function only was employed for subsequent analysis.

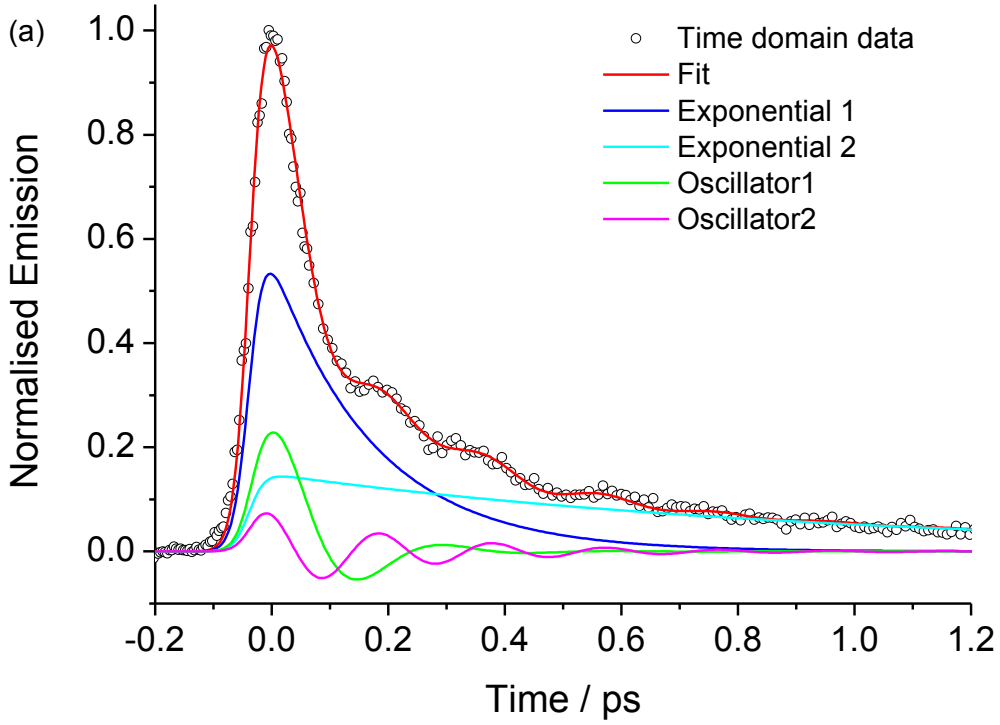

Figure S2(a) – The individual components of the fit to the time domain data (emission measured at 556 nm). The fitting function is comprised of the sum of two exponential decay terms and two damped harmonic oscillators. The faster damping of the larger amplitude oscillator is evident.

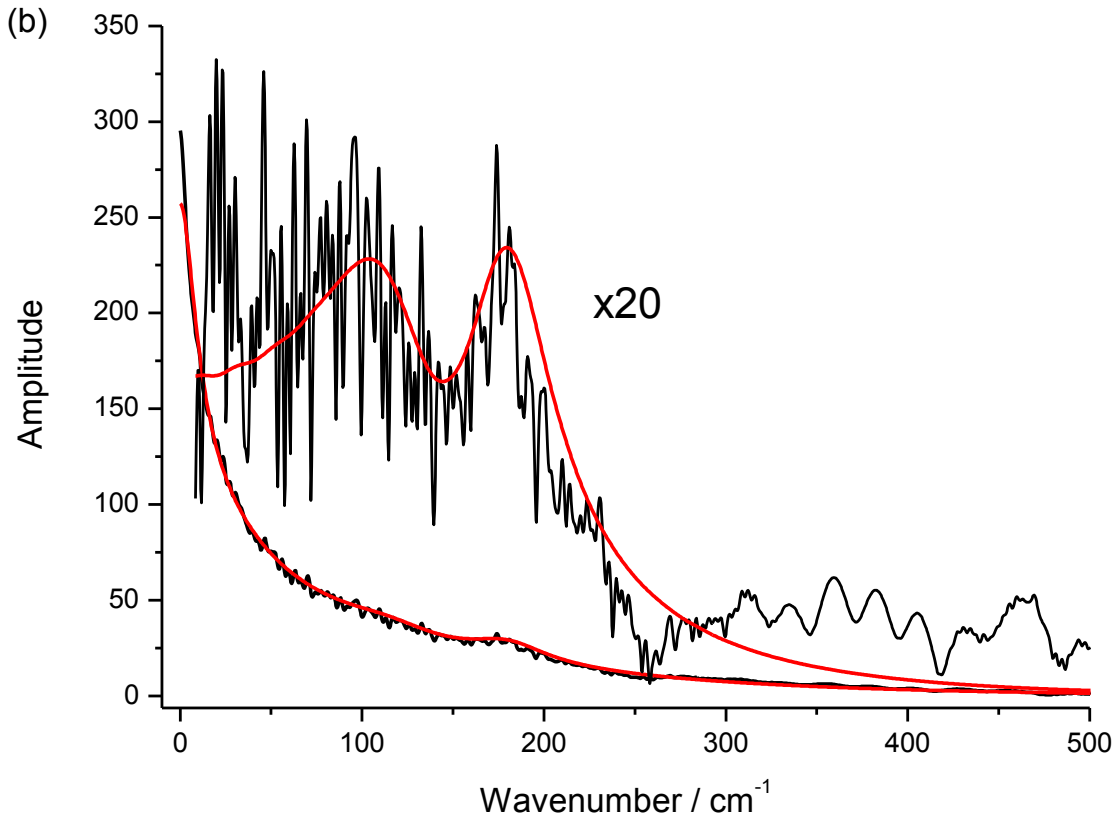

Figure S2(b) – Fourier transform of the time domain data (emission measured at 535 nm). Raw time domain data (black) are compared to fitted data (red). The Fourier transform of the time domain data is dominated at low frequency by a Lorentzian lineshape. This is due to the ultrafast exponential decay in the time domain. In order to resolve the time domain oscillation in the frequency domain, the exponential decay components were subtracted, leaving only the oscillatory parts. The Fourier transform of this (shown magnified x20) resulted in two distinct bands. The red line is the Fourier transform of the two oscillatory components recovered from the time domain fitting (113 cm^{-1} and 180 cm^{-1}). The low signal to noise at low frequency reflects the absence of signal at long times in the subtracted data. No filtering has been applied.

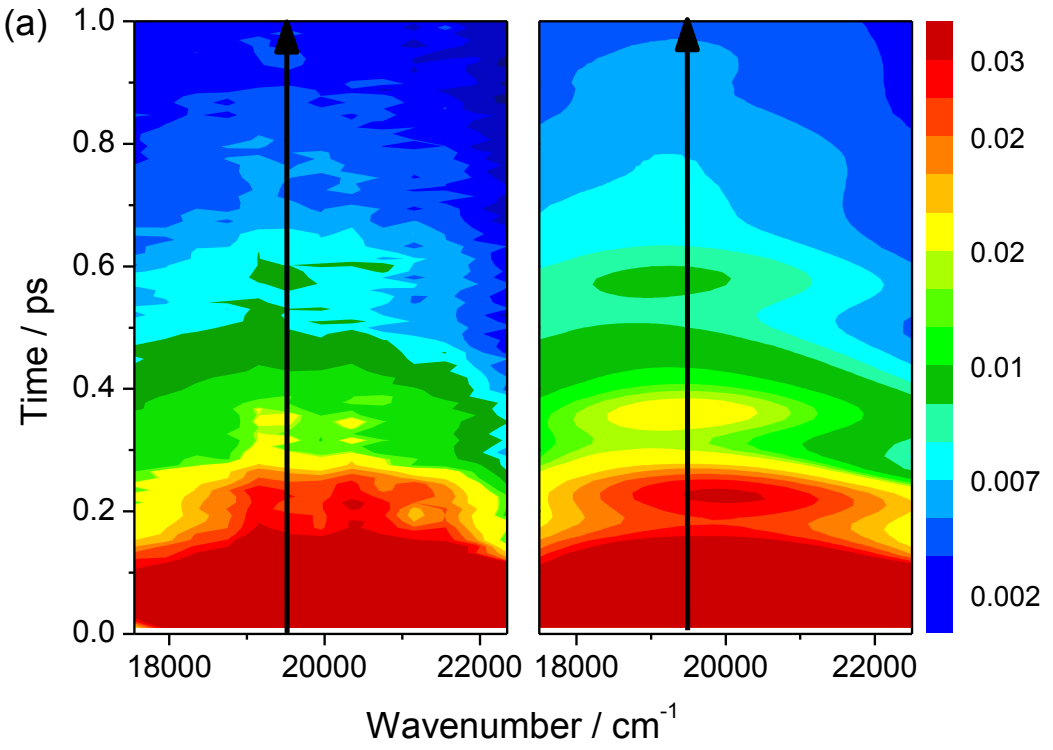

Figure S3a – A comparison of the raw experimental data points (left) and the log-normal fit to the deconvoluted data (right). The experimental data clearly shows the oscillation which is made clearer by the deconvolution fitting procedure described. The black arrows represent a single frequency slice (19760 cm^{-1}) of both surfaces to allow a direct comparison of the experimental and fitted data in figure S3b.

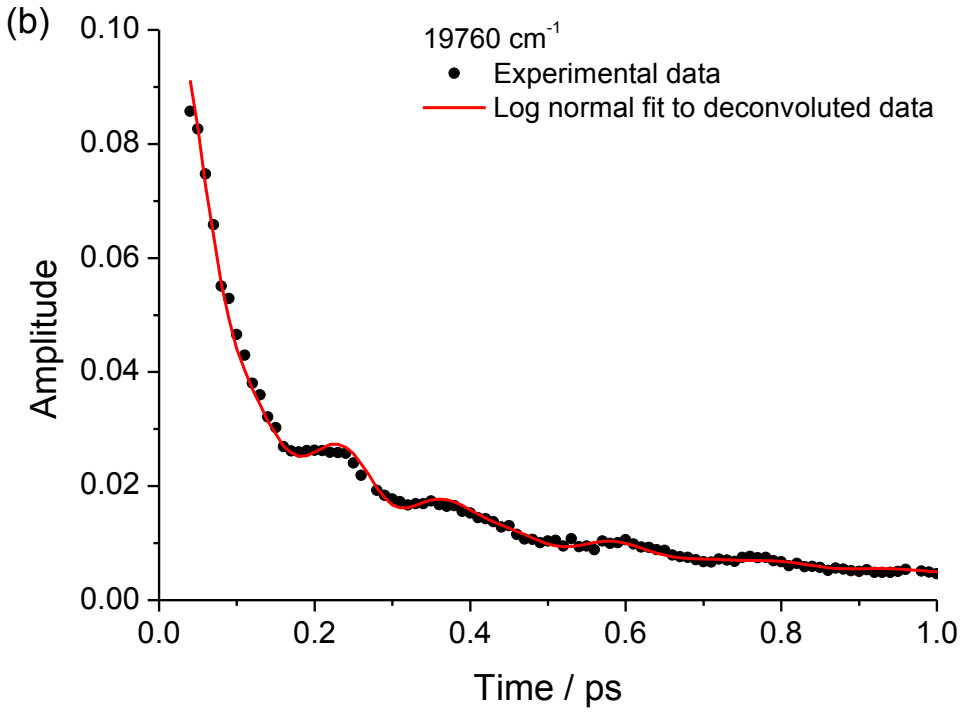

Figure S3b – A comparison of the experimental data (black dots) and the log-normal fit to the deconvoluted data (red line) at 19760 cm^{-1}. The two data sets are in excellent agreement, clearly showing that the oscillation observed is not an artefact introduced by the analysis procedure, but is a real feature of the experimental data.

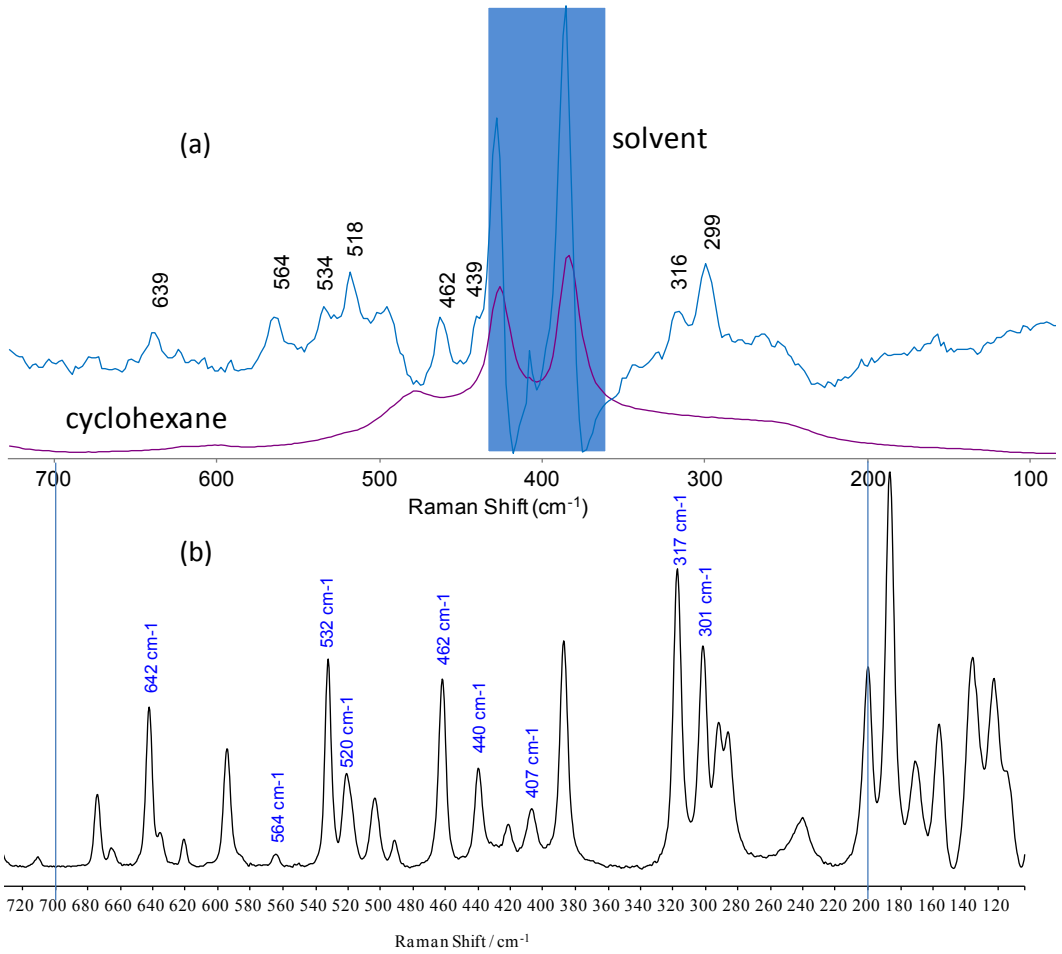

Figure S4a (a) Ground state resonance Raman Spectrum of **1** in cyclohexane (blue) recorded with 355 nm excitation and recovered after subtraction of the solvent Raman spectrum (shown in magenta). The shaded region shows where subtraction is imperfect and hence the assignment of the signals is unreliable. Cyclohexane was chosen as solvent because Raman active modes of DCM obscure even more of the critical low frequency region; in solvent free regions there was a perfect correspondence between the spectra recorded in DCM and in cyclohexane. There are no obvious features in the ground state spectrum to match the excited state modes observed in the time resolved fluorescence. However, two enhanced modes are apparent near 300 cm^{-1}. (b) The experimental non resonant Raman spectrum of crystalline **1** shows that two modes at low frequency (317 cm^{-1} and 301 cm^{-1}) match the resonantly enhanced ground state modes (316 cm^{-1} and 299 cm^{-1}). In addition C=C stretch modes at

higher frequency (not shown) were also enhanced. There is a mode matching the minor higher frequency excited state mode (180 cm^{-1}), but it is not observed as resonantly enhanced.

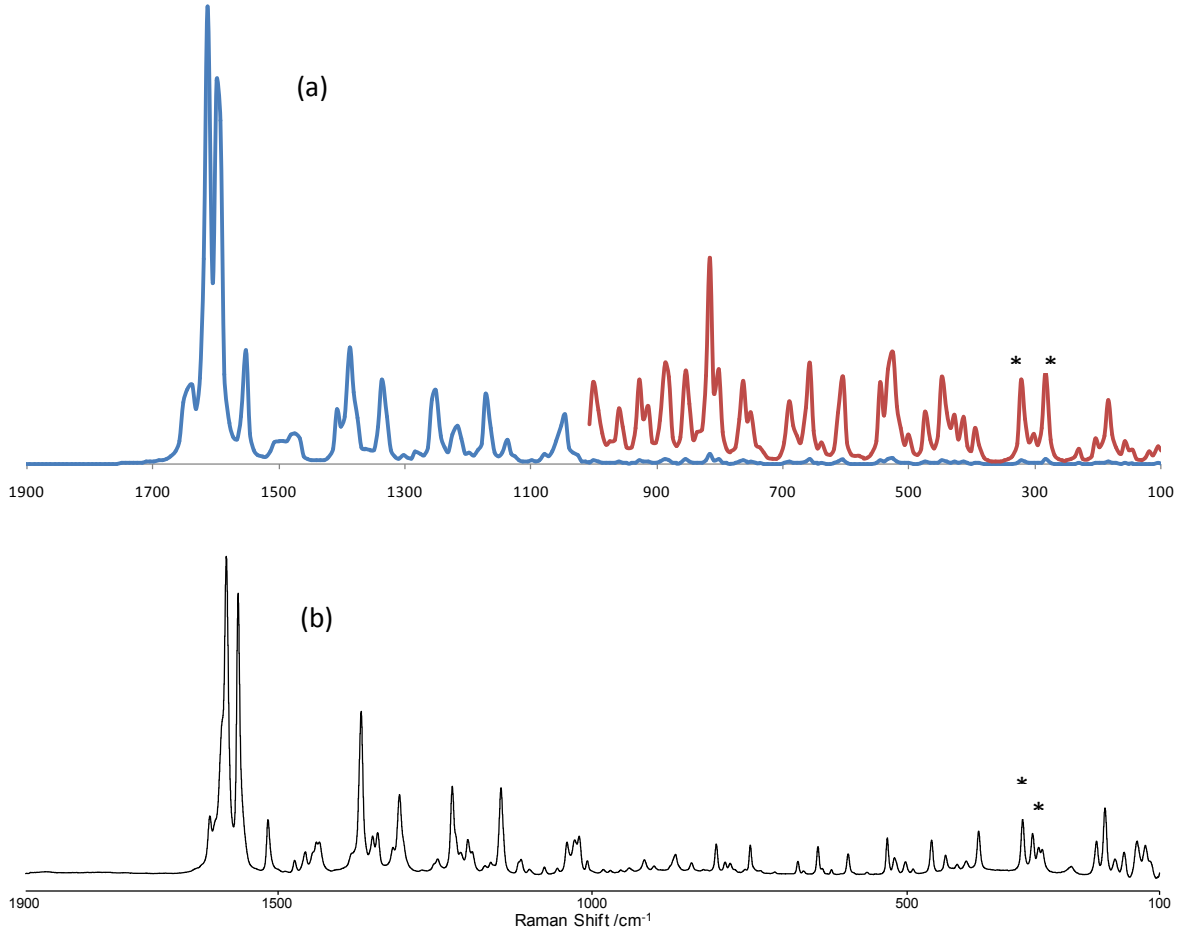

Figure S4b (a) The Raman spectrum of **1** calculated[1] from DFT (corresponding to an isolated molecule environment) is compared with the non resonant Raman spectrum of **1** (crystalline powder). The low frequency part shown in red has been amplified. (b) The experimental off resonance Raman spectrum of **1**. The low-frequency modes matching the frequencies enhanced in the resonance Raman spectrum are marked with an asterisk. Agreement between calculated and experimental spectra is good. The low frequency modes seen in the experimental spectrum but absent from the calculations may indicate contributions from lattice modes.

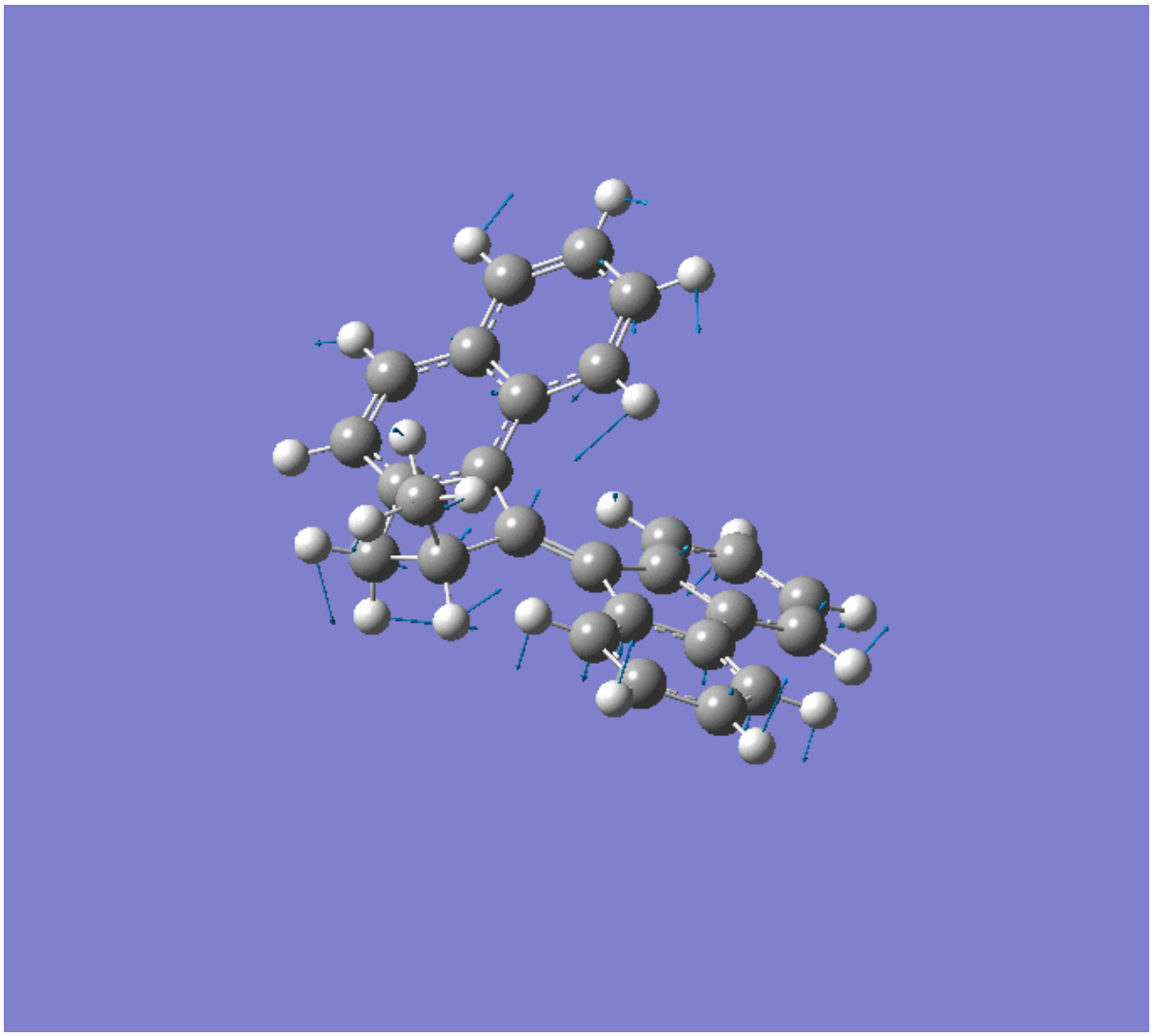

Figure S4c Displacements for the mode observed in Resonance Raman (299 cm^{-1}) were calculated for the matching 301 cm^{-1}. Out of place activity around C9 is observed. The motion is not specifically pyramidalization (which is calculated at 392 cm^{-1}, obscured in Figure S4a by solvent modes). Neither experimental nor calculated ground state modes match the frequencies observed in the excited state. The absence of such a correspondence is commonly observed (see main text).

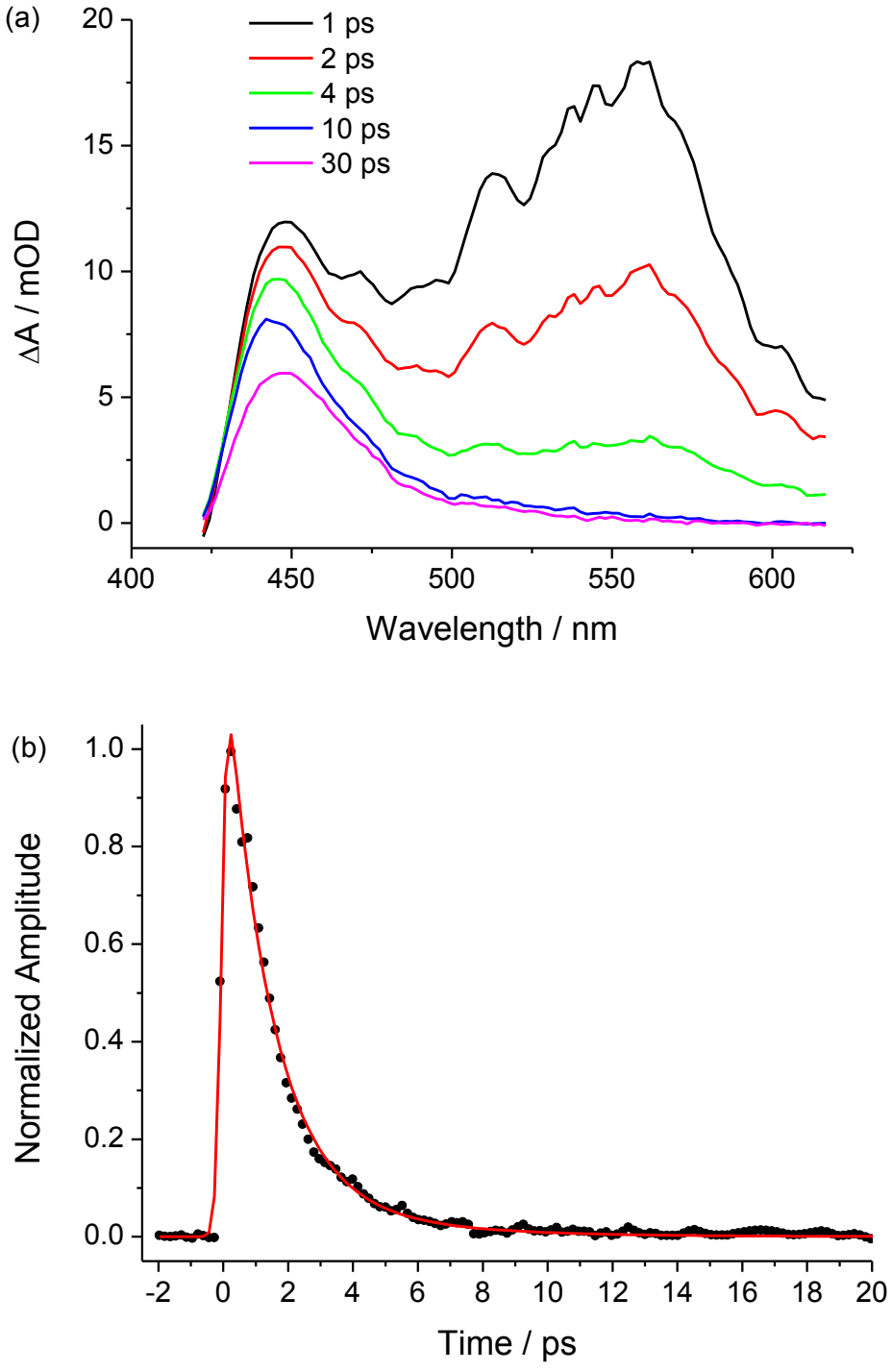

Figure S5 Preliminary transient absorption data for **1** in DCM, reported as a function of time after excitation at 400 nm. (a) A transient absorption/stimulated emission feature centred at 560 nm decays away within 10 ps. In addition there is a transient near 450 nm with more complex kinetics including a long lived (i.e. much longer than 20 ps) component. This higher energy transient probably contains multiple contributions, from the excited state absorption,

the ground state bleach and the hot ground state reached after the internal conversion. (b) The relaxation time of the 560 nm transient was measured as 1.5±0.3 ps. This relaxation time is consistent with the longer, relaxed, component observed in the time resolved fluorescence, and thus suggests an assignment to the relaxed excited state. Calculations suggest that this state has already undergone substantial structural change compared to the Franck Condon state.

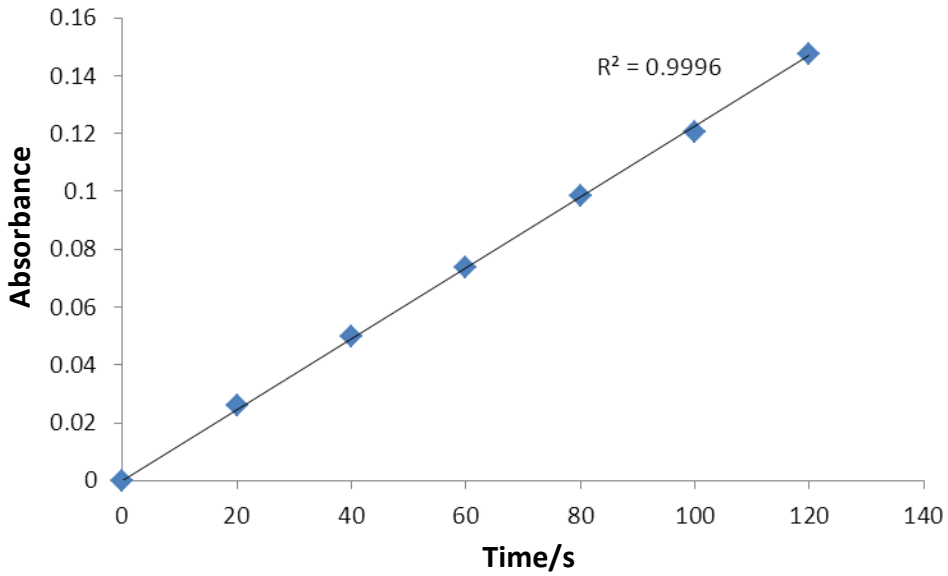

Figure S6 Absorption (475 nm) of a toluene solution of **1** followed over time when irradiated at 365±1 nm (blue diamonds) and linear fit (black line). These data were utilised for the quantum yield measurement.

References

(1) M. J. Frisch, G. W. T., H. B. Schlegel, G. E. Scuseria, M. A. Robb, J. R. Cheeseman, J. A. Montgomery, Jr., T. Vreven, K. N. Kudin, J. C. Burant, J. M. Millam, S. S. Iyengar, J. Tomasi, V. Barone, B. Mennucci, M. Cossi, G. Scalmani, N. Rega, G. A. Petersson, H. Nakatsuji, M. Hada, M. Ehara, K. Toyota, R. Fukuda, J. Hasegawa, M. Ishida, T. Nakajima, Y. Honda, O. Kitao, H. Nakai, M. Klene, X. Li, J. E. Knox, H. P. Hratchian, J. B. Cross, C. Adamo, J. Jaramillo, R. Gomperts, R. E. Stratmann, O. Yazyev, A. J. Austin, R. Cammi, C. Pomelli, J. W. Ochterski, P. Y. Ayala, K. Morokuma, G. A. Voth, P. Salvador, J. J. Dannenberg, V. G. Zakrzewski, S. Dapprich, A. D. Daniels, M. C. Strain, O. Farkas, D. K. Malick, A. D. Rabuck, K. Raghavachari, J. B. Foresman, J. V. Ortiz, Q. Cui, A. G. Baboul, S. Clifford, J. Cioslowski, B. B. Stefanov, G. Liu, A. Liashenko, P. Piskorz, I. Komaromi, R. L. Martin, D. J. Fox, T. Keith, M. A. Al-Laham, C. Y. Peng, A. Nanayakkara, M. Challacombe, P. M. W. Gill, B. Johnson, W. Chen, M. W. Wong, C. Gonzalez, and J. A. Pople *Gaussian 03, Revision A.1,Gaussian, Inc., Pittsburgh PA,* **2003**.

(2) Zhao, R.-K.; Lukacs, A.; Haigney, A.; Brust, R.; Greetham, G. M.; Towrie, M.; Tonge, P. J.; Meech, S. R. *Physical Chemistry Chemical Physics* **2011**, *13*, 17642-17648.